Journal of Hydroscience and Hydraulic Engineering
Vol. 3, No. 1, April, 1985, pp.23-43.

# TURBULENT STRUCTURE OF CURRENTS UNDER THE ACTION OF WIND SHEAR

By

Hiroichi Tsuruya

Port and Harbour Research Institute,
Ministry of Transport,
Yokosuka 239, Japan

## SYNOPSIS

Measurements of turbulent currents under the action of wind shear are presented. In the experiment, V-type wedge shaped hot-film anemometer is used in order to measure the turbulent fluctuations in longitudinal and vertical components simultaneously. Modification of mean current distribution, characteristic properties of turbulent motions and diffusion coefficients have been discussed.

When wind blows on adverse current, turbulent fluctuations and diffusion coefficient increase near the water surface. On the contrary, near the middle of the flow, they decrease compared with the case of current only. This is closely related to the mean velocity distributions.

A method of estimating the turbulent intensities and vertical diffusion coefficient in the case that adverse wind shear acts on the water surface is proposed.

## INTRODUCTION

Turbulence plays an important role in the transport processes in the ocean. Energy, mass and momentum are transported across the air-sea interface which is exposed to the wind shear and surface waves. In the ocean, turbulence is produced both directly from the interfacial stress by the wind and indirectly by the rate of momentum loss from the surface waves by such process as wave breaking (Phillips (15)).

In the coastal region, currents such as tidal currents, local wind-generated currents and wave-generated currents are usually observed. Interaction of waves or wind shear and currents is important in many applications. Deformation of surface waves by currents has been investigated by many researchers (e.g., see Peregrine and Jonsson (14)). On the contrary, turbulence of the water flow interacting with waves or wind shear has not been studied sufficiently. A few experimental investigations have been made on the alteration of the mean and turbulent flow parameters due to the wave interactions (e.g., see van Hoften and Karaki (20); Kemp and Simons (6,7)). As far as I know, however, no study has been made on the turbulent structure of currents under the action of wind shear.

This paper describes experiments carried out in a laboratory wind-wave tunnel, to investigate the turbulent structure of open-channel flow under the action of wind shear in which wind waves are suppressed. In particular, changes induced in the mean velocity profiles, turbulent intensities and spectra, and diffusion coefficient are investigated.

## EXPERIMENTAL EQUIPMENTS AND PROCEDURES

The experiments were conducted in a wind-wave tunnel, whose sketches are shown in Figs. 1(a) and 1(b). The dimensions of the test section are 2850 cm long, 150 cm wide, 130 cm deep. The side walls consist of glass plates. A wind blower is located on the windward (right hand) side of the test section over the waterway, and wind is generated by an axial fan driven by a 50 kW variable speed motor. The

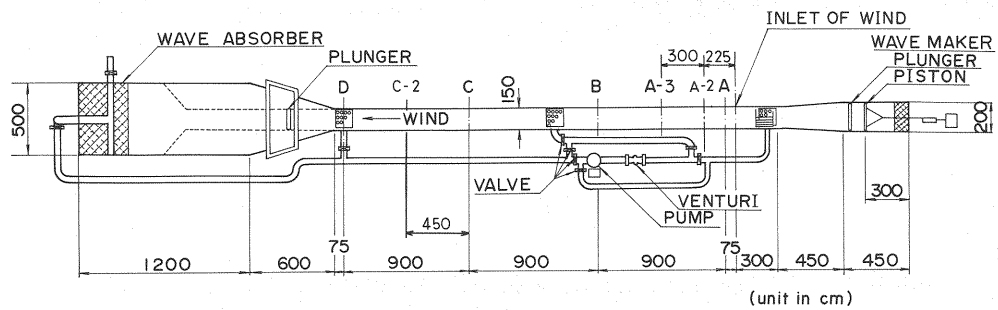


Fig. 1 (a)

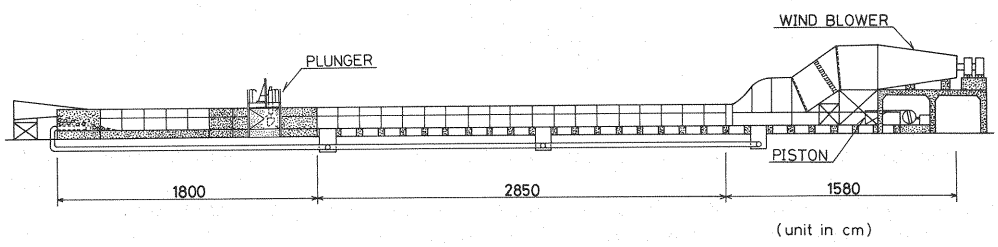


Fig. 1 (b)

Fig. 1 Wind-wave tunnel

wind tunnel is fitted with guide vanes, a fine mesh screen and honeycombs in order to provide uniform velocity profiles. The wind speed is set up by regulating the rotational speed of the fan.

The water currents are generated by a pump and a pipeline system. Current direction in the flume can be controlled by the operation of valves. In the present experiments the flow rate was adjusted accurately by means of a venturimeter and a manometer. If the reading of the differential pressure head of manometer exceeds ±1mm from the setting value, the flow rate was readjusted.

On the leeward, the width of the test section is enlarged in order to diffuse winds. In this part wooden walls are installed.

The characteristics of the turbulent motion and the diffusion coefficients are much complicated in the situation where wind waves and currents both exist. In order to simplify the phenomenon and to examine the contributions of wind shear alone to the mean velocity distribution, turbulent motion and the diffusion coefficient, the present series of experiments were conducted with wind waves being suppressed by the application of detergent ($C_{12}H_{25}OSO_3Na$) to the water. By a preliminary test, it was confirmed that detergent of 1.8kg or 24.5ppm concentration was sufficient to suppress the wind waves in the flume. It was decided to keep the water depth at the measuring section constant at 45 cm.

The revolutions of the wind blower was kept constant at 300 rpm. In this case the free-stream wind velocity near the inlet of wind was 8.1 m/s. Wind velocities over the water surface were measured with a pitot static tube and a MKS BARATRON type 310BH differential pressure head and type 170M-6B electronic unit. The mean water flow velocity was set at 23.8 and 30.3 cm/s. Measurements of current velocity were made with a DISA type 55R72 wedge-shaped V-type hot film anemometer at various elevations at the stations A and B. In the experiment the V-probe was attached to a self-elevating system which could be raised and lowered a distance of 110 cm with a setting accuracy of 0.1 mm. The anemometer was operated at an overheat ratio of 1.05. It was calibrated by towing it at constant speed within still water in a calibration tank. The carriage speed was determined by measuring the time that it took traverse a 1 m length of the tank. The probe was carefully cleaned by using a small brush before each measurement. The experimental conditions are summerized in Table 1.

The surface drift current velocity was estimated by measuring the time of

floats passing two stations 30 cm upwind and downwind from the test section respectively. Thin circular papers of 0.56 cm diameter punched from computer cards, saturated with paraffin, were used as surface floats.

A digital data recorder (DATAC-2000B, Iwatsu Electronic Co.,Ltd.) was used for recording the output signals from the measuring instruments on the on-line basis. The sampling time interval of turbulent velocities was $\Delta t=1/102.4$ s and the total data number N=16384. Some of the data were sampled at $\Delta t=1/204.8$ s and the total data number N=32768. Consequently the time of measurement in both cases were 160 s exactly.

Table 1 Experimental conditions

| Case | Station | $U_a$ (m/s) | $U_w$ (cm/s) |
|---|---|---|---|
| S-1 | A | 8.1 | 23.8 |
| S-2 | | | 30.3 |
| S-3 | B | | 23.8 |

## WIND VELOCITY PROFILE

Figure 2 shows the wind velocity profiles at stations A,A-2,B,C and D.

The mean velocity profiles near the air-water interface follow a logarithmic distribution

$$U_a(z)=\frac{u_{*a}}{\kappa}\ln\frac{z}{z_{0a}} \qquad (1)$$

where $U_a(z)$=wind velocity at an elevation z above the mean water surface; $u_{*a}(=\sqrt{\tau_a/\rho_a})$ = friction velocity of the wind; $\tau_a$ = wind shear stress at the water surface; $\rho_a$ = density of air; $\kappa$ = von Kármán constant usually taken to be 0.4; and $z_{0a}$ = roughness length.

Generally, shear stress $\tau$ in the fluid is related to the friction velocity $u_*$ by the following relation

$$\tau = \rho u_*^2 \qquad (2)$$

where $\rho$ = density of the fluid. As it has been well confirmed that the velocity distribution near the wall or water surface follow the logarithmic distribution as shown by Eq. 1, we can estimate the friction velocity $u_*$ by applying Eq. 1 to the measured data.

The friction velocities $u_{*a}$ were estimated by applying Eq. 1 to the measured data. They are 29.2, 27.8, 29.0, 27.1 and 34.3 cm/s for the stations A, A-2, B, C and D,respectively. The roughness parameter $z_{0a}$ and eddy viscosity $\nu_a$ of the wind are $2.946\times10^{-4}$ cm and 0.148 $cm^2/s$ at the station A.

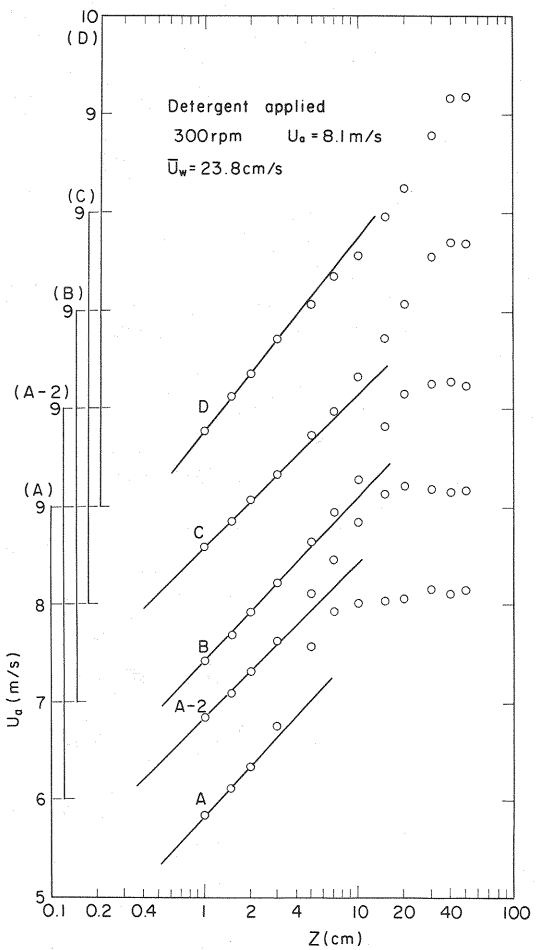


Fig. 2 Wind profiles over the water surface. Abscissa is shifted successively for different fetches

## CURRENT VELOCITY DISTRIBUTION

The coordinate system to be used here is that shown in Fig. 3. For convenience, however, the wind direction is considered to be positive only in the theoretical calculations of mean velocity distributions which will be presented later.

Measured mean velocity distributions of currents with and without wind are shown in Figs. 4, 5 and 6. They correspond to the cases S-1, S-2 and S-3, respectively and the experimental conditions have already been shown in Table 1. In order to examine the influence of detergent to the mean velocity distribution, velocity measurements without wind were made for both with and without detergent (Fig. 4). Although there is some scatter in the case of detergent applied, no significant effect can be found.

In open-channel flow, the well known velocity distributions are logarithmic and 1/7-th power laws. Logarithmic law has the same form as Eq. 1 and the mean velocity distribution for open-channel flow can be expressed as

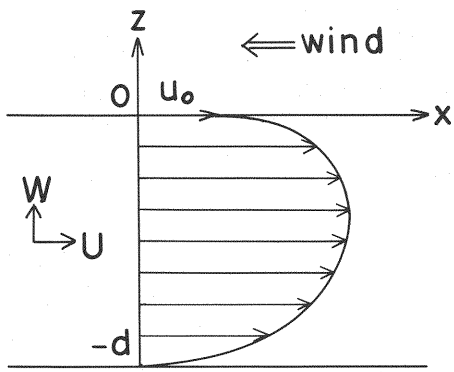


Fig. 3 Coordinate system

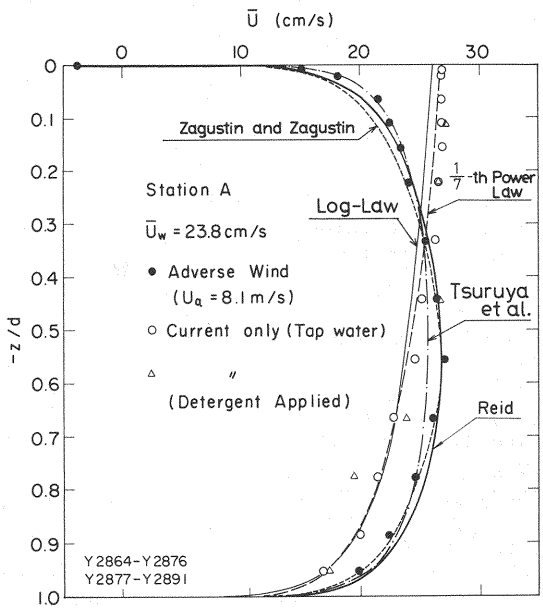


Fig. 4 Current profiles (Station A, $\bar{U}_w$ = 23.8 cm/s)

$$\bar{U}(z) = \frac{u_{*b}}{\kappa} \ln \frac{z+d}{z_{0b}} \qquad (3)$$

where $\bar{U}(z)$ = mean velocity at an elevation z; $u_{*b}$ = friction velocity at the bottom; $z_{0b}$ = roughness length at the bed; and d = depth of water. Friction velocity and the roughness length were estimated from the observed velocity distribution near the bed. The relation 3 is represented in Figs. 4, 5 and 6. As the value of -z/d decreases

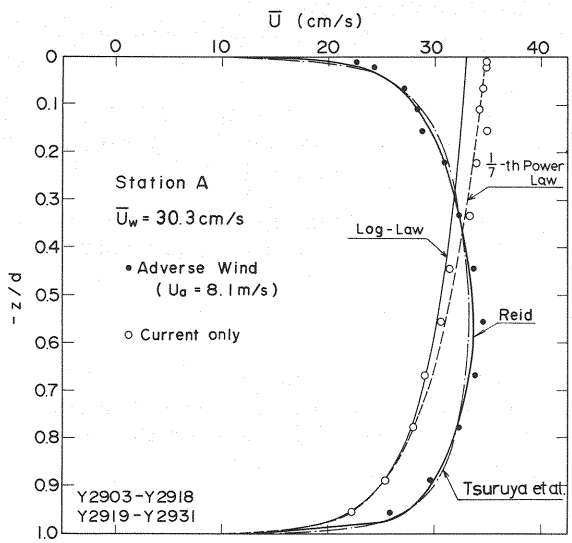


Fig. 5 Current profiles (Station A, $\bar{U}_w$ = 30.3 cm/s)

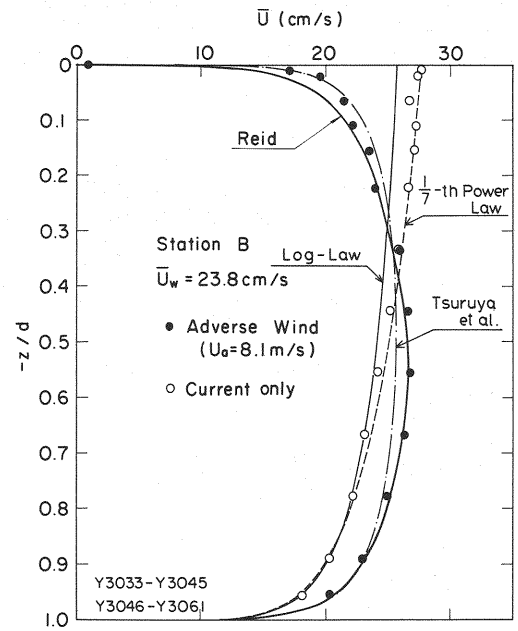


Fig. 6 Current profiles (Station B, $\bar{U}_w$ = 23.8 cm/s)

(in the upper layer of the flow), the difference between the experimental data and Eq. 3 becomes remarkable.

The 1/7-th power law is

$$\bar{U}(z) = u_0 \left(\frac{z+d}{d}\right)^{1/7} \tag{4}$$

where $u_0$ = surface velocity. In the figures, Eq. 4 is represented as broken lines. For all cases the agreement between experimental data and the 1/7-th power law is better than for the logarithmic distribution.

The velocity distribution in an open-channel turbulent flow in the presence of a surface wind stress has been investigated by Reid (16) and Tsuruya et al. (18). The theories will be explained in order.

Reid (16) derived the generalized formula for velocity profile which takes the influence of surface stress into account making use of Montgomery's (10) generalization of the Prandtl-von Kármán's mixing length theory. Its theoretical derivation is outlined below.

According to Prandtl's one-dimensional mixing-length theory (e.g., see Hinze (4)), the shear stress at the elevation z can be represented as follows

$$\tau = \rho_w \ell^2 \left|\frac{d\bar{U}(z)}{dz}\right| \frac{d\bar{U}(z)}{dz} \tag{5}$$

where $\rho_w$ = density of water; and $\ell$ = mixing length.

For the case of flow in a wide channel with a free surface, the generalized mixing length hypothesis of Montgomery (10) leads to the following quadratic form for the mixing length

$$\ell = \frac{\kappa}{d}(d+z+z_{0b})(z_{0w}-z) \tag{6}$$

where $z_{0b}$ = characteristic roughness length for the channel bed; and $z_{0w}$ = similar characteristic parameter for the free surface. Near the surface and the bottom Eq. 6 reduces to the well known relation $\ell = \kappa z$.

Next, the shear stress within the flow is assumed to have a linear distribution. If $\tau_s$ is the shear stress at the free surface and $\tau_b$ the bottom stress, the shear stress $\tau$ can be represented as

$$\tau = \tau_s \frac{d+z}{d} - \tau_b \frac{z}{d} \tag{7}$$

in which x axis is taken to the direction of $\tau_s$. The velocity distribution for the adverse current condition can be obtained by integrating Eq. 5 making use of Eqs. 6 and 7 as

$$\frac{\bar{U}(z)}{u_{*w}} = -U_m - \frac{1}{\kappa}\left[B_0 \ln\frac{B_0 - y}{B_0 + y} + 2B_1 \tan^{-1}\frac{y}{B_1}\right], \quad \zeta < \zeta_m \tag{8}$$

$$\frac{\bar{U}(z)}{u_{*w}} = -U_m - \frac{1}{\kappa}\left[2B_0 \tan^{-1}\frac{y}{B_0} + B_1 \ln\frac{B_1 - y}{B_1 + y}\right], \quad \zeta > \zeta_m \tag{9}$$

$$U_m = \frac{1}{\kappa}\left[B_0 \ln\frac{B_0 + \sqrt{|m|}}{B_0 - \sqrt{|m|}} - 2B_1 \tan^{-1}\frac{\sqrt{|m|}}{B_1}\right] \tag{10}$$

$$m = \frac{\tau_b}{\tau_s}$$

$$\zeta = \frac{d+z}{d}$$

$$\left.\begin{aligned}
\zeta_m &= \frac{|m|}{1+|m|} \\
y &= \sqrt{|m+(1-m)\zeta|} \\
B_0 &= \sqrt{|(1-m)r_0 - m|} \\
B_1 &= \sqrt{|1+(1-m)r_1|} \\
\kappa' &= \kappa(1+r_0+r_1) \\
r_0 &= \frac{z_{0b}}{d} \\
r_1 &= \frac{z_{0w}}{d}
\end{aligned}\right\} \qquad (11)$$

where $u_{*w}$ = friction velocity of the water flow at the free surface; $\tau_s (= \rho_w u_{*w}^2)$ = shear stress at the water surface; and $\tau_b$ = shear stress at the bed.

If $r_0, r_1 << 1$ and $m < 0$ the surface velocity $u_0$ can be approximated from Eq. 9, namely,

$$\frac{u_0}{u_{*w}} = \frac{1}{\kappa}\left[\ln\frac{4}{(1+|m|)r_1} + 2\tan^{-1}\sqrt{|m|} - \sqrt{|m|}\left\{\ln\frac{4|m|}{(1+|m|)r_0} + 2\tan^{-1}\frac{1}{\sqrt{|m|}}\right\}\right] \qquad (12)$$

The mean current velocity $\bar{U}_w$ is defined as

$$\bar{U}_w = \frac{1}{d}\int_{-d}^{0} \bar{U}(z)\,dz \qquad (13)$$

The substitution of Eqs. 8 and 9 in the integral of Eq. 13 leads to

$$\frac{\bar{U}_w}{u_{*w}} = \frac{2}{\kappa}\left[1+\sqrt{|m|} - B_0\left\{\tan^{-1}\frac{1}{B_0} + \frac{1}{2}\ln\frac{B_0+\sqrt{|m|}}{B_0-\sqrt{|m|}}\right\}\right] \qquad (14)$$

If the mean velocity is specified for the given m and $\tau_s$, the bed roughness length $z_{0b}$ can be obtained from Eq. 14. The parameters employed in calculating Eqs. 8 and 9 are summerized in Table 2 for Figs. 4, 5 and 6. Thick solid curves which are named as 'Reid' in these figures represent the calculated results making use of Eqs. 8 and 9, but the sign is reversed. The reason that we adopt $m = -0.8$ is based on the experimental data of the Reynolds stress and this will be discussed later. The calculated curves nearly fit to the observed data. Near the water surface and the bottom, however, they indicate slight difference. In the calculation, $u_{*w}$ was estimated so that the calculated curve shows a best fit to the experimental data.

Tsuruya et al. (18) obtained the velocity distribution of the drift current,

Table 2 Parameters in calculating Eqs. 8 and 9

| Station | $\bar{U}_w$ (cm/s) | m | $u_0$ (cm/s) | $u_{*w}$ (cm/s) |
|---|---|---|---|---|
| A | -23.8 | -0.8 | 3.84 | 1.30 |
| | -30.3 | -0.8 | -3.70 | 1.41 |
| B | -23.8 | -0.8 | -0.85 | 1.30 |

assuming that the logarithmic profile can stand near the water surface and the bottom, that is

$$\bar{U}(z) = \frac{u_{*w}}{\kappa} \ln \frac{z_{0w} + d}{z_{0w} - z} - \frac{u_{*b}}{\kappa} \ln \frac{d + z_{0b} + z}{z_{0b}} \tag{15}$$

From Eq. 15 mean velocity $\bar{U}_w$ is represented as

$$\bar{U}_w \simeq \frac{u_{*w}}{\kappa} - \frac{u_{*b}}{\kappa} \left( \ln \frac{d}{z_{0b}} - 1 \right) \tag{16}$$

If it can be assumed that the bottom is smooth, the logarithmic distribution of the velocity gives

$$\frac{z_{0b} u_{*b}}{\nu_w} = 0.111 \tag{17}$$

where $\nu_w$ = kinematic viscosity of water. The surface roughness length $z_{0w}$ can be obtained by assuming that the roughness Reynolds number just above and below the water surface are equal, that is

$$z_{0w} = \sqrt{\frac{\rho_w}{\rho_a} \frac{\nu_w}{\nu_a}} z_{0a} \tag{18}$$

where $\nu_a$ = kinematic viscosity of air. If $u_0$, $z_{0w}$ and $\bar{U}_w$ are known, $u_{*w}$, $u_{*b}$ and $z_{0b}$ are obtained by solving Eqs. 16, 17 and 18. The results are indicated as dash-dot lines in Figs. 4, 5 and 6. Although there is some difference at the center of the stream, the agreement is good near the surface and the bottom. The values of parameters employed and estimated in calculating the velocity distributions are summerized in table 3. The estimated values of $u_{*w}$ in Table 3 are less than that in Table 2.

Table 3 Parameters in calculating Eq. 15

| Station | $\bar{U}_w$ (cm/s) | $u_0$ (cm/s) | $u_{*a}$ (cm/s) | $z_{0a} \times 10^4$ (cm) | $\nu_a$ (cm$^2$/s) | $z_{0w} \times 10^4$ (cm) | $u_{*w}$ (cm/s) | $u_{*b}$ (cm/s) | $z_{0b} \times 10^4$ (cm) |
|---|---|---|---|---|---|---|---|---|---|
| A | -23.8 | 3.84 | 29.18 | 2.95 | 0.158 | 5.31 | 1.17 | 1.10 | 9.89 |
| | -30.3 | -3.70 | | | | 11.1 | 1.25 | 1.35 | 8.08 |
| B | -23.8 | -0.85 | 29.04 | 5.69 | 0.156 | 5.31 | 0.99 | 1.09 | 10.7 |

Because both estimation contain many assumptions, it is not certain for the present that which is more reasonable. In the later analysis, however, the values of $u_{*w}$ in Table 2 will be used.

The velocity distribution of the flow with adverse wind is similar to that in the pipe flow. Next, we try to apply the theory obtained for the pipe flow to the present problem. Zagustin and Zagustin (21) studied the turbulent flow in a smooth pipe using a "balance of pulsation energy" equation. They obtained an expression for the universal law of the velocity distribution

$$\frac{U-u}{u_*} = 5.0 \tanh^{-1} \left( \frac{r}{R} \right)^{3/2} \tag{19}$$

where U = velocity at the axis of the pipe; u = velocity at a given point in the pipe; $u_*$ = friction velocity; r = radial distance measured from the axis of the pipe; and R = radius of the pipe. If we regard the current in this experiment having the same mean flow characteristics as a pipe flow, the relation 19 can be used by separating the flow field into two regions at the height where the velocity gradient diminishes. This condition is satisfied when $-z/d = 0.555$. The calculated distribution using the

Zagustin and Zagustin's theory is represented in Fig. 4. In the upper layer, the theoretical curve is small compared with the experimental data.

## REYNOLDS STRESS

Turbulent motion may be defined as a randomly fluctuating motion superimposed on a mean motion. Instantaneous velocity is then given by

$$U = \bar{U} + u$$
$$W = \bar{W} + w \qquad (20)$$

where $\bar{U}$, $\bar{W}$ ( $=0$ ) = mean velocities and u, w = turbulent motions in x and z directions, respectively.

The Reynolds stress $\tau$ and the intensities of the turbulent motions can be written as

$$\tau = -\rho_w \overline{uw} \; ; \quad u'^2 = \overline{u^2} \; ; \quad w'^2 = \overline{w^2} \qquad (21)$$

where u', w' = root-mean-square components in x and z directions, respectively. From the first equation of 21, the shear velocity $u_*$ can be written as $u_*^2 = -\overline{uw}$.

Figure 7 shows the measured Reynolds stress normalized by a surface shear velocity in the case of adverse wind. In the middle part of the flow, three cases lie close to the one linear distribution. The height at which the Reynolds stress becomes zero is $-z/d = 0.555$. If we assume that the Reynolds stress follow a linear distribution, it can be considered from figure that the bottom shear stress is about 80% of the surface shear stress. This is the reason why we adopt $m = -0.8$ in the calculation of Reid's distribution.

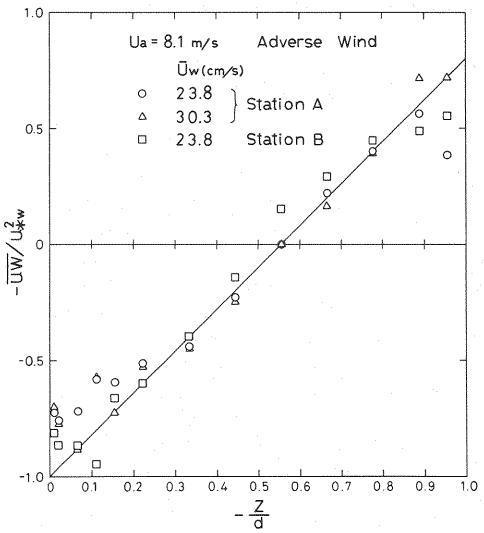


Fig. 7 Reynolds stress normalized by surface shear velocity

The conditional sampling technique as discribed below is used to investigate the detailed characteristics of the Reynolds stress. The u-w plane is devided into five regions as shown in Fig. 8. In this figure, the hatched region is called as a 'hole', and is bounded by the curves $|uw| = \text{constant}$. A parameter H is introduced to satisfy the relation $|uw| = H|\overline{uw}|$ ( Nakagawa and Nezu (11) ). The parameter H is called the hole size after Lu and Willmarth (8).

The contributions to $\overline{uw}$ from the four quadrants are computed from the following equations;

$$\langle uw \rangle_{i,H} = \lim_{T\to\infty} \frac{1}{T} \int_0^T u(t)w(t)D_{i,H}[u(t),w(t)]dt \; ; \quad (i=1,2,3,4) \qquad (22)$$

where $\langle\rangle$ represents the conditional sampling and

$$D_{i,H}(u,w) = \begin{cases} 1, & \text{if } |uw| > H|\overline{uw}| \text{ and the point}(u,w) \text{ in the i-th quadrant} \\ 0, & \text{otherwise} \end{cases} \qquad (23)$$

The contribution rate from the each quadrant to the Reynolds stress is therefore

$$S_{i,H} = \langle uw \rangle_{i,H} / \overline{uw} \tag{24}$$

The contribution to $\overline{uw}$ from the 'hole' region is obtained from

$$S_{5,H} = \frac{1}{\overline{uw}} \lim_{T\to\infty} \frac{1}{T} \int_0^T u(t)w(t)D_{5,H}[u(t),w(t)]dt \tag{25}$$

where

$$D_{5,H}(u,w) = \begin{cases} 1, & \text{if } |uw| \leq H|\overline{uw}| \\ 0, & \text{otherwise} \end{cases} \tag{26}$$

These five contributions are all functions of the hole size and must satisfy the following relation

$$\sum_{i=1}^{4} S_{i,H} + S_{5,H} = 1 \tag{27}$$

The time fraction during which each contribution is being made is

$$T_{i,H} = \lim_{T\to\infty} \frac{1}{T} \int_0^T D_{i,H}[u(t),w(t)]dt\,; \quad (i = 1,2,3,4,5) \tag{28}$$

where $D_{i,H}$ is represented by Eqs. 23 and 26. It is customary to label the events defined by the four quadrants i as outward interactions (i = 1; u>0, w>0), ejections (i = 2; u<0, w>0), inward interactions (i = 3; u<0, w<0) and sweeps (i = 4; u>0, w<0), respectively.

Figure 9 represents the fractional contributions from different events at the elevation z = -40cm in the case of current only. The directions of the line segments of open squares in the figure represent the quadrants to which squares belong as illustrated in the caption of Fig. 9. In this figure, contributions from the second (ejection) and the fourth (sweep) quadrants are remarkable as usually seen in the boundary layer flow. The theoretical curves by Nakagawa and Nezu (11) are also represented in the figure. When wind acts on the water surface, contributions from the first and the third quadrants dominate near the water surface (see Fig. 10). It can be deduced from the figure

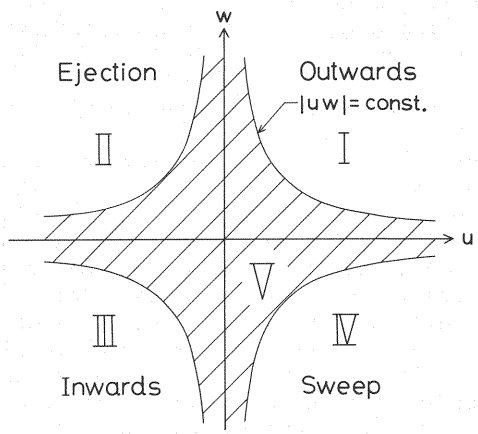


Fig. 8 Sketch of 'Hole' region in the u,w plane

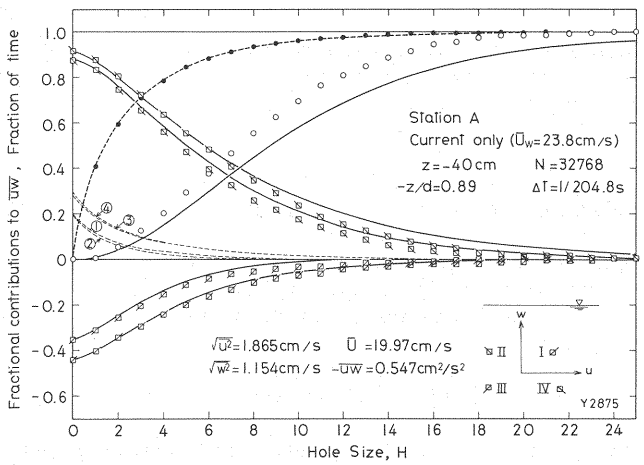


Fig. 9 Contributions to $\overline{uw}$ from different events (Station A, current only, $\bar{U}_w$ = 23.8 cm/s, z = -40 cm). ⓘ, fraction of time occupied by i-th event. Observed values; $S_{1,H}$:⊠, $S_{2,H}$:⊠, $S_{3,H}$:⊠, $S_{4,H}$:⊠, $S_{5,H}$:○, $T_{5,H}$:●. ——,----:calculated curves by Nakagawa and Nezu's theory

that the water surface which suffers the wind shear resembles like a wall. Boundary layer develops from the water surface and in this situation, the contributions from the third and the first quadrants can be considered as ejections and sweeps, respectively, provided that the water surface is considered as a wall. Near the water surface, the contributions from the third quadrant is slightly greater than that from the first quadrant.

## TURBULENCE INTENSITIES AND SPECTRA

When detergent is applied, the water properties are slightly varied. For example, surface tension decreases to a value of 70% of tap water and wind waves cannot develop under the action of wind even at relatively high wind speed. Eddy viscosity was also measured but significant difference could not be recognized. As it is suspected that the detergent influences the turbulent structures, turbulent spectra are examined in a detergent added water. In the same manner as the mean current distribution, frequency spectra of turbulent fluctuations in the cases with and without detergent are compared. Figure 11 shows the frequency spectra of u components in the cases with and without detergent. Both cases yield the same spectra. This means that the influence of the detergent can be ignored in turbulent streams. In the following discussions, therefore, we consider that the detergent have nothing to do with the structures of turbulence intensities and spectra. In this section we investigate an universal relation of turbulent intensities under the action of wind and the characteristics of the spectrum of turbulence.

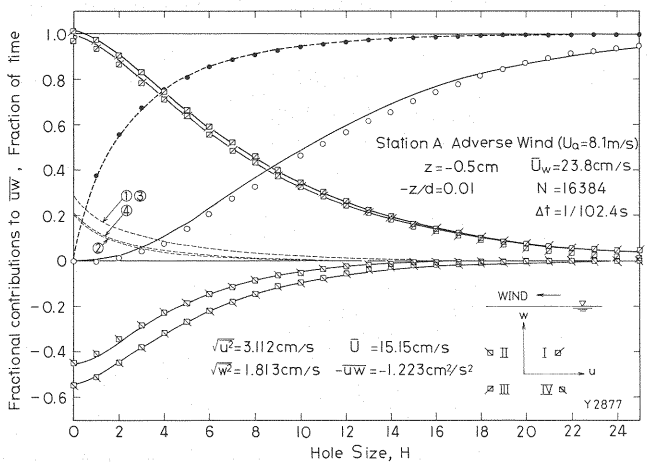


Fig. 10 Contributions to $\overline{uw}$ from different events (Station A, adverse wind, $\bar{U}_w = 23.8$ cm/s, $z = -0.5$ cm), Notation as in Fig. 9

In Figs. 12 and 13, relative turbulence intensities $u'/\bar{U}$ and $w'/\bar{U}$ for the case S-1 are represented. In the figures the data of McQuivey and Richardson (9) are also plotted. It is evident that in the case of current only, distributions of both u and w components resemble like the data of McQuivey and Richardson. Near the water surface, however, the difference for the u components becomes noticeable. As experiments by McQuivey and Richardson were conducted in an open-channel with 3 cm water depth, it can be considered that the difference between our data and that of McQuivey and Richardson is originated from the variation of the influence of surface fluctuations which is called as "inactive component" (Bradshaw (1)). In the present experiment, water depth was 45 cm and no significant surface fluctuations could be observed.

Nezu (12) has studied the turbulence

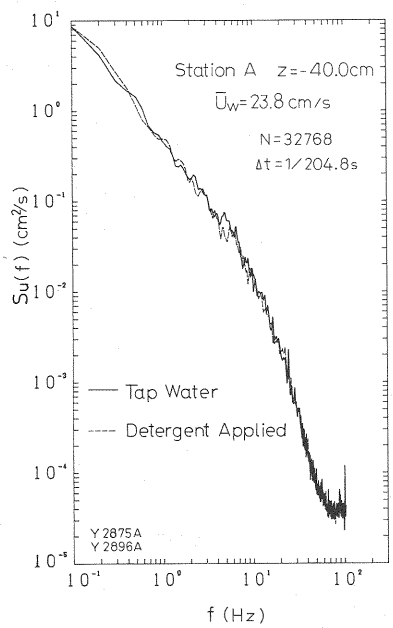


Fig. 11 Longitudinal turbulence spectra (Tap water and detergent applied)

intensities in an open channel flow and found the universal distributions of turbulence intensities non-dimensionalized by the shear velocity $u_{*b}$ at the bed.

They are represented as

$$u'/u_{*b} = D_1 \exp(-\lambda\zeta/2) \; ; \quad D_1 = 2.30$$
$$w'/u_{*b} = D_2 \exp(-\lambda\zeta/2) \; ; \quad D_2 = 1.27 \qquad (29)$$

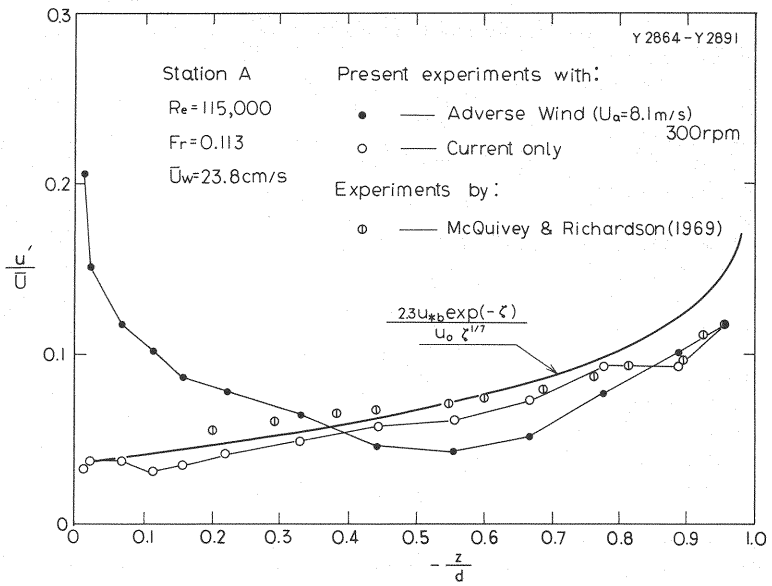


Fig. 12 Longitudinal turbulence intensities
(Station A, $\bar{U}_w = 23.8$ cm/s)

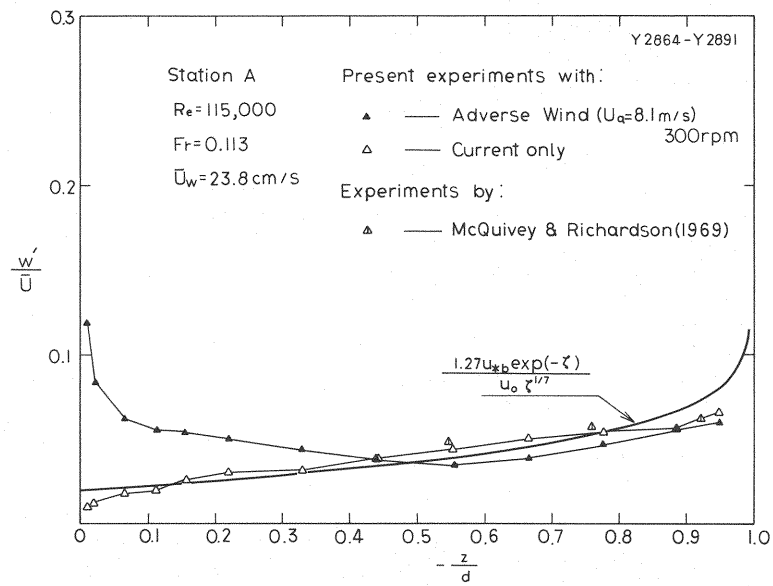


Fig. 13 Vertical turbulence intensities
(Station A, $\bar{U}_w = 23.8$ cm/s)

where u',w' = root-mean-square turbulence-velocity components; $\lambda$ = constant and is taken to be 2.0 after Nezu; and $\zeta = (d+z)/d$.

Now we use the 1/7-th power law as a mean velocity distribution. With the aid of Eq. 29, the relative turbulence intensities can be written as

$$\frac{u'}{\bar{U}} = \frac{2.3u_{*b}\exp(-\zeta)}{u_0\zeta^{1/7}}$$
$$\frac{w'}{\bar{U}} = \frac{1.27u_{*b}\exp(-\zeta)}{u_0\zeta^{1/7}} \qquad (30)$$

Equations 30 are represented in Figs. 12 and 13 as solid curves. Except near the bottom ($-z/d = 1.0$), the agreement between the Nezu's universal functions 29 and our experimental data is fairly good.

When adverse wind acts on the surface of the stream, turbulence intensities near the water surface increase compared with the case of current only. On the other hand, they decrease where the relative depth $-z/d$ is higher than 0.4. Turbulence production by the Reynolds stress can be represented as

$$-\rho_w\overline{uw}\frac{d\bar{U}}{dz} \qquad (31)$$

From Fig. 7 it is seen that the Reynolds stress at the elevation $-z/d = 0.55$ is zero. As a result, the turbulence produced by the Reynolds stress would be very small near $-z/d = 0.55$. This can be confirmed in Fig. 12.

When wind blows on the water surface, the development of turbulence from the surface can be considered to have the same form as that from the bottom as represented in Eq. 29. Consequently, the turbulence intensities can be written as

$$u'^2 = G_{1b}{}^2u_{*b}{}^2\exp(-\lambda_1\zeta) + G_{1w}{}^2u_{*w}{}^2\exp\{\lambda_1'(\zeta-1)\} \qquad (32.a)$$

$$w'^2 = G_{2b}{}^2u_{*b}{}^2\exp(-\lambda_2\zeta) + G_{2w}{}^2u_{*w}{}^2\exp\{\lambda_2'(\zeta-1)\} \qquad (32.b)$$

It was assumed that the turbulence intensities from the water surface and from the bottom can be added linearly. Moreover we assume that the constants are the same as Nezu's constants $D_1$ and $D_2$, namely, $G_{1b} = G_{1w} = 2.3$, $G_{2b} = G_{2w} = 1.27$. Furthermore, assuming $\lambda_1 = \lambda_1'$ and $\lambda_2 = \lambda_2'$ and making use of the experimental data, $\lambda_1$ and $\lambda_2$ can be obtained as

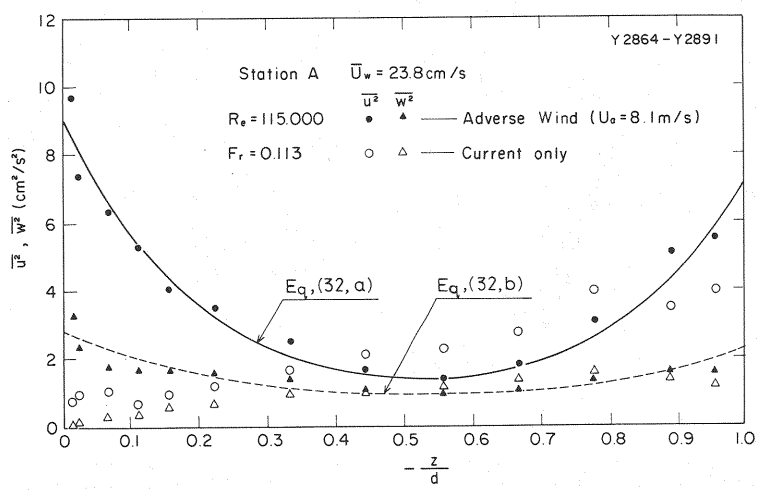


Fig. 14 Mean square values of velocity fluctuations (Station A, $\bar{U}_W$ = 23.8 cm/s)

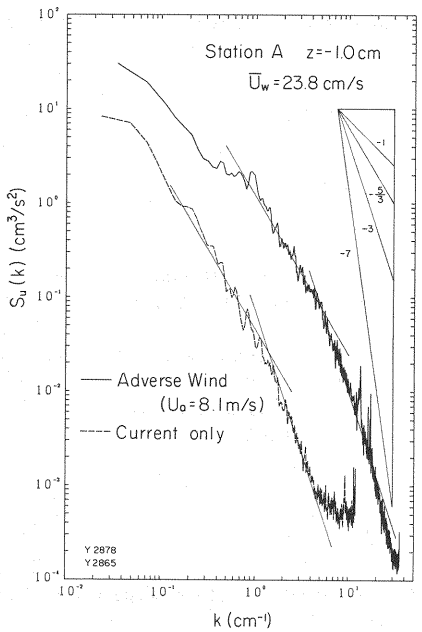


Fig. 15 Longitudinal wave number spectra with current only and adverse wind (Station A, z = -1 cm, $\bar{U}_w$ = 23.8 cm/s)

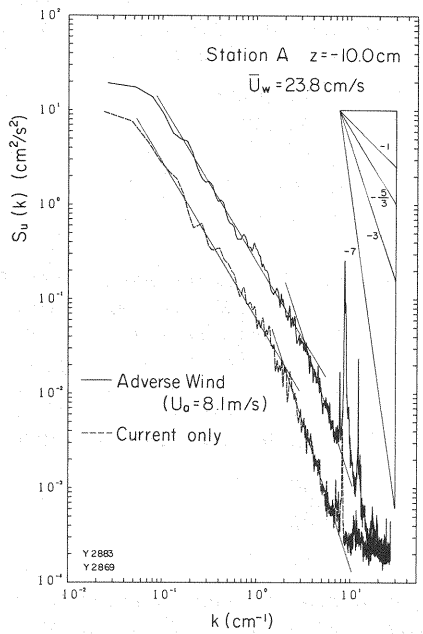


Fig. 16 Notation as in Fig. 15, (z = -10 cm)

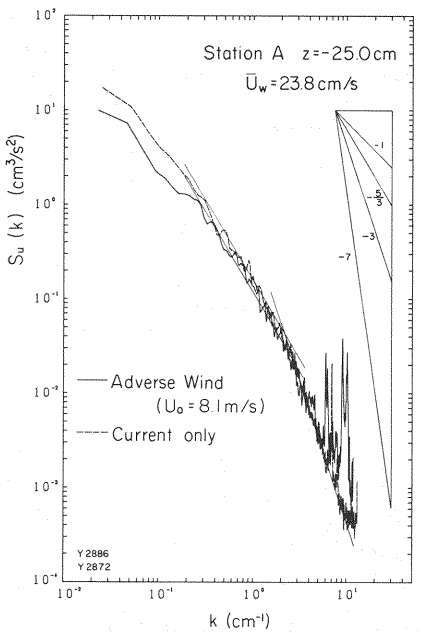


Fig. 17 Notation as in Fig. 15, (z = -25 cm)

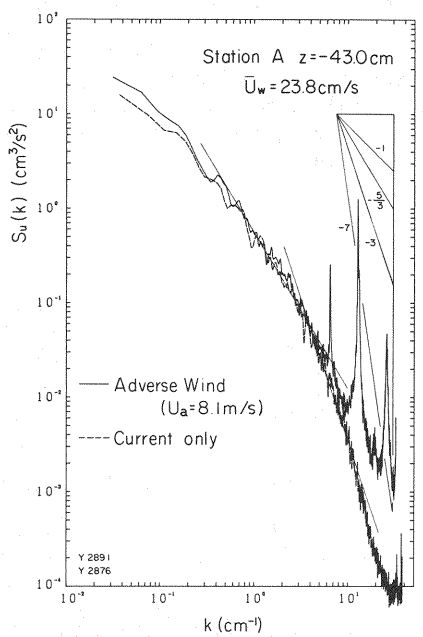


Fig. 18 Notation as in Fig. 15, (z = -43 cm)

$$\lambda_1 = 4.86$$
$$\lambda_2 = 3.37 \qquad (33)$$

In Fig. 14 calculated curves (32 a, b) are shown as solid and broken curves for u and w components, respectively. The agreement is fairly good. In the calculation, $u_{*b} = 1.15$ cm/s and $u_{*w} = 1.3$ cm/s were used.

The one-dimensional power-spectral density function was computed using the FFT algorithm. And all the frequency spectra of u components are converted into wave number spectra. Some of them are shown in Figs. 15∿18. They correspond to the case S-1. Near the water surface, spectral components in the case of adverse wind are exceedingly greater than that in the case of current only. On the contraly, in the middle part of the flow (-25>z>-35 cm), spectral components in the case of current only are slightly greater than that in the case of adverse wind. This corresponds to the fact that near $-z/d = 0.555$, turbulence intensities take the lowest values as we have already shown in Figs. 12 and 13. Near the bottom, turbulent spectra are not so affected by the wind.

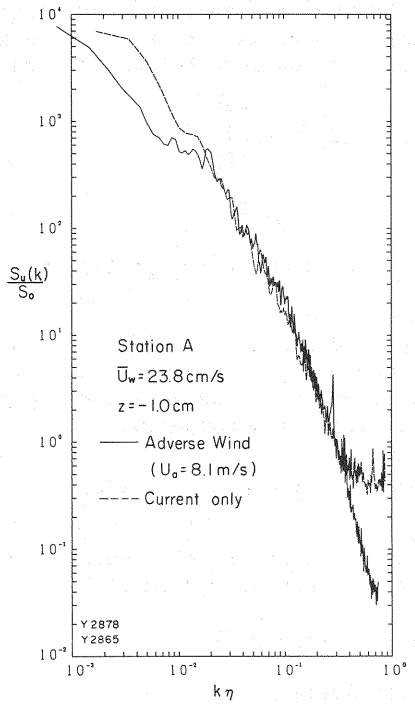


Fig. 19 Normalized energy spectra (z = -1 cm)

According to the previous studies in open-channel flow, the spectrum of turbulence has an universal form (e.g., Nezu (12)). For simplicity, we consider the one-dimensional energy spectrum S(k) in the wave number field k, where $k = 2\pi f/\bar{U}$, f and $\bar{U}$ are frequency and mean current velocity, respectively. For the large Reynolds numbers, the form of S(k) in the inertial subrange can be expressed as

$$S(k) = A\varepsilon^{2/3}k^{-5/3} \qquad (34)$$

where $\varepsilon$ = dissipation rate by turbulence per unit mass; and A = absolute constant.

In the viscous dissipation range, Inoue (5) has obtained the relation as follows

$$S(k) \propto \varepsilon\nu^{-1}k^{-3} \qquad (35)$$

where $\nu$ = kinematic viscosity of the fluid. Heisenberg (see for example, Hinze (4)), on the other hand, has obtained another relation as follows

$$S(k) = \frac{2}{63}\cdot\left(\frac{\alpha}{2}\right)\cdot(\varepsilon\nu^5)^{1/4}\cdot\left(\frac{k}{k_d}\right)^{-7} \qquad (36)$$

where $\alpha$ = constant of proportionality; $k_d = 1/\eta$; and $\eta = (\nu^3/\varepsilon)^{1/4}$ is the Kolmogoroff length scale. In Figs. 15∿18 the shapes of spectra are remarkably similar and each spectra has the -5/3 law for the inertial subrange and the -3 law for the viscous dissipation range.

The coordinates are non-dimensionalized using $S_0 = (\varepsilon\nu_w^5)^{1/4}$ and the Kolmogoroff length scale $\eta$, where $\nu_w$ = kinematic viscosity of water. Figure 19 shows an example of the normalized wave number spectra. Each spectrum collapses to a single curve except at the low wave numbers. This figure corresponds to the Fig. 15. This indicates that in the case of adverse wind, the relations 34 and 35 can hold the same as in the case of usual open channel flow.

## DIFFUSION COEFFICIENT

In the case that the turbulence is homogeneous and stationary, i.e., if the average properties are uniform in space and steady in time, Taylor (17) obtained the expression for the mean square $\overline{Z^2}$ of a large number of samples

$$\frac{d\overline{Z^2}}{dt} = 2\overline{w_L^2}\int_0^t {}_wR_L(\tau)\,d\tau \tag{37}$$

and

$$\overline{Z^2}(T) = 2\overline{w_L^2}\int_0^T\int_0^t {}_wR_L(\tau)\,d\tau dt \tag{38}$$

where $Z$ = distance traversed by a particle in time $T$; $\overline{w_L^2}$ = Lagrangian mean-square turbulence-velocity component in z direction; and ${}_wR_L(\tau)$ = Lagrangian autocorrelation coefficient. The subscript w represents that the autocorrelation coefficient is calculated for w component. Integration of Eq. 38 by parts gives

$$\overline{Z^2}(T) = 2\overline{w_L^2}\int_0^T (T-\tau)\,{}_wR_L(\tau)\,d\tau \tag{39}$$

The coefficient ${}_wR_L(\tau)$ should be unity when $\tau = 0$ and effectively zero for large $\tau$, say $\tau > t_1$. Hence, for small T

$$\overline{Z^2}(T) = \overline{w_L^2}T^2 \tag{40}$$

and for large T

$$\overline{Z^2}(T) = 2T_L\overline{w_L^2}T \tag{41}$$

where $T_L$ is a constant time-scale of turbulence and defined by

$$T_L = \int_0^\infty {}_wR_L(\tau)\,d\tau \tag{42}$$

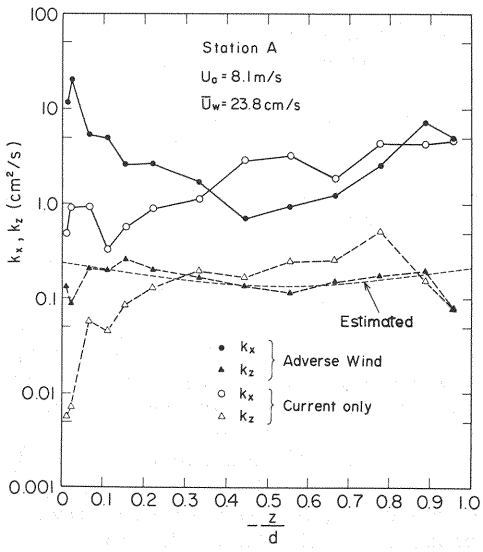


Fig. 20 Eulerian diffusion coefficient (Station A, $\bar{U}_w$ = 23.8 cm/s)

The flux F of the property across a fixed surface due to the turbulent motion is effectively defined by the following relation

$$F = -K(T)\frac{\partial C}{\partial z} \tag{43}$$

where $K(T)$ = diffusion coefficient; and $\partial C/\partial z$ = gradient, normal to the surface, of the concentration of the property undergoing diffusion.

The diffusion coefficient $K(T)$ has the dimension of [length×velocity] and can be represented as the average of the multiplication of the velocities and displacements of fluid particles which transport any diffusible property. Thus, the diffusion coefficient is expressed as

$$K(T) = \overline{w_L Z} = \overline{Z\frac{dZ}{dT}} = \frac{1}{2}\frac{d\overline{Z^2}}{dT} \tag{44}$$

From Eqs. 37 and 44 the diffusion coefficient can be written as

$$K(T) = \overline{w_L^2}\int_0^{t_1} {}_wR_L(\tau)d\tau \tag{45}$$

where $t_1$ = value of $\tau$ beyond which ${}_wR_L(\tau)$ remains zero. On the basis of observations in the atmosphere, Hay and Pasquill (2) concluded that the Lagrangian correlation fell off much more slowly than did the autocorrelation of the velocity component measured at a fixed point, and in their later study (3) they adopted a simple hypothesis of the following:

$${}_wR_L(\xi) = {}_wR_E(t) \quad ; \quad \text{when } \xi = \beta t \tag{46}$$

where the subscript E refferring to the Eulerian autocorrelation coefficient from measurements at a fixed point and $\beta$ is the ratio of the Lagrangian to the Eulerian time scales.

Consequently, the relation

$$\int_0^{\infty} {}_wR_L(\xi)d\xi = \beta\int_0^{\infty} {}_wR_E(t)dt \tag{47}$$

can be obtained.

From the observations of the crosswind spread of particles and simultaneous measurements of the fluctuations of wind speed, they summerized the average value of $\beta$ as being 4 with a "scatter range" from 1.1 to 8.5 for the diffusion over short distances in the atmosphere. The error in the estimation of $\beta$ will often not be serious. If the true value is $\beta$, and the value assumed is $\beta'$, it is easily seen that the value of $\sqrt{\overline{Z^2}}$ derived will be $(\beta'/\beta)^q$ times the true value, where q will vary from zero when T is small to a maximum of 0.5 when T is large (Pasquill (13)). Therefore, $\beta$ is assumed as unity in the present study.

Eulerian diffusion coefficient in both longitudinal and vertical directions were calculated using Eqs. 45 and 47. The results are illustrated in Fig. 20. Near the water surface, diffusion coefficients in both x and z directions increase in the case of adverse wind compared with that of current only. Figure 21 shows the ratio of the diffusion coefficients $K_x$, $K_z$ in the case of adverse wind to $K_{x0}$, $K_{z0}$ in the case of current only. The ratio increase up to 20 near the surface. On the contrary, this ratio becomes less than unity in the range of $0.3<-z/d<0.85$. The tendency is similar to the distribution of turbulence intensities.

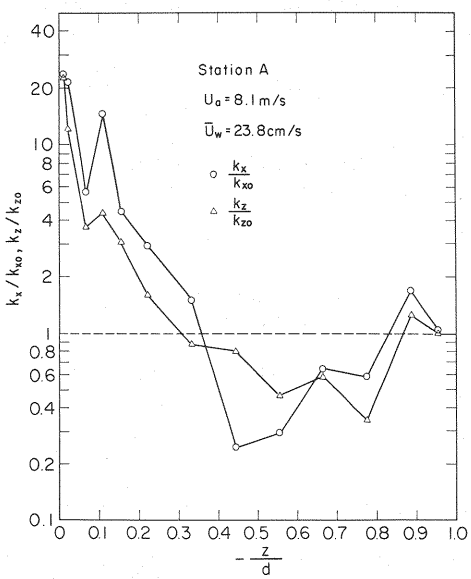


Fig. 21 Ratio of adverse wind to current only diffusion coefficient

Eddy diffusivity $K_z$ can be interpreted as the multiplication of the characteristic length and the velocity. If we choose the mixing length $\ell_z$ as the characteristic length and the root-mean-square of turbulence $\sqrt{\overline{w^2}}$ as the velocity, eddy diffusivity $K_z$ can be represented as

$$K_z = \ell_z\sqrt{\overline{w^2}} \tag{48}$$

In general, $\ell_z$ may be the function of the location and the flow conditions. In practical use, however, it will be very useful if $\ell_z$ does not change appreciably

over the entire range of the flow.

We examined the value of $\ell_z$ and it was found that in the case of adverse wind, $\ell_z$ was nearly constant. The relative value of $\ell_z$ to the water depth was $\ell_z/d \simeq 3.2 \times 10^{-3}$. Using this value as the mixing length and making use of Eqs. 32.b and 48, vertical diffusion coefficient $K_z$ was calculated and is illustrated in Fig. 20 as a broken line. The vertical diffusion coefficient can be estimated by such a simple way, but the longitudinal diffusion coefficient cannot be obtained easily because the mixing length is a function of the location.

## CONCLUSIONS

Turbulent fluctuations and velocity profiles have been investigated in the flow field under the action of wind. Contributions of wind to the turbulent structures and velocity profiles have been discussed together with the Eulerian diffusion coefficient.

The following conclusions can be drawn from the present study:

1. When wind blows over the adverse current, turbulent fluctuations and diffusion coefficients in both longitudinal and vertical components increase near the water surface. On the contrary, they decrease near the central region of the flow.

2. The mean velocity profile is deformed by the action of wind shear. Consequently, in the case of adverse current, a gradient of velocity profile vanish near the center of the flow and turbulent production by the Reynolds stress also vanish causing the decrease of turbulence intensities and diffusion coefficient.

3. Mean velocity profile of adverse current under the action of wind shear can be approximately represented by both Reid's theory and author's equation.

4. A method of estimating the turbulent intensities and vertical diffusion coefficient in adverse current under the action of wind is proposed.

## ACKNOWLEDGEMENTS

The author wishes to thank Dr. Y. Goda, the Deputy Director General, for his critical reading of the manuscript and valuable comments. The author also wishes to express his appriciation to Mr. S. Nakano, member of Hydrodynamics Laboratory, for his valuable discussions, and to Mr. H. Terakawa, Y. Matsunobu and H. Ichinohe, for conducting the experiments and drawing the figures.

## REFERENCES

1. Bradshaw, P. : 'Inactive' motion and pressure fluctuations in turbulent boundary layers, J. Fluid Mech., Vol.66, pp.241-258, 1967.
2. Hay, J.S. and F. Pasquill : Diffusion from a fixed source at a height of a few hundred feet in the atmosphere, J. Fluid Mech., Vol.2, Part 3, pp.299-310, 1957.
3. Hay, J.S. and F. Pasquill : Diffusion from a continuous source in relation to the spectrum and scale of turbulence, Atmospheric diffusion and air pollution, Advances in Geophysics, Vol.6, pp.345-365, Academic Press, 1959.
4. Hinze, J.O. : Turbulence, 2nd ed.,McGraw-Hill, 1975.
5. Inoue, E. : On the smallest turbulon in a turbulent fluid, Rept. Inst. Sci. and Tech., Univ. of Tokyo, Vol.4, No.7.8, pp.194-200, 1950, (in Japanese).
6. Kemp, P.H. and R.R. Simons : The interaction between waves and a turbulent current: waves propagating with the current, J. Fluid Mech., Vol.116, pp.227-250, 1982.
7. Kemp, P.H. and R.R. Simons : The interaction of waves and a turbulent current: waves propagating against the current, J. Fluid Mech., Vol.130, pp.73-89, 1983.
8. Lu, S.S. and W.W. Willmarth : Measurements of the structure of the Reynolds stress in a turbulent boundary layer, J. Fluid Mech., Vol.60, pp.481-511, 1973.
9. McQuivey, R.S. and E.V. Richardson : Some turbulence measurements in open-channel flow, Proc. ASCE, HY-1, pp.209-223, 1969.

10. Montgomery, R.B. : Generalization for cylinders of Prandtl's linear assumption for maxing length, Annals N. Y. Academy of Sciences, Vol.44, Art.1, 1943.
11. Nakagawa, H and I. Nezu : Prediction of the contributions to the Reynolds stress from bursting events in open-channel flows, J. Fluid Mech., Vol.80, part 1, pp. 99-128, 1977.
12. Nezu, I. : Basic research on the turbulent structure of open-channel flows, Doctoral thesis presented to Kyoto Univ., 118p., 1977, (in Japanese).
13. Pasquill, F. : Atmospheric Diffusion, D. van Nostland Company Ltd., 1962.
14. Peregrine, D.H. and I.G. Jonsson : Interaction of waves and currents, Miscellaneous Rept. No.83-6, U.S. Army, Corps of Eng., 88p., 1983.
15. Phillips, O.M. : The Dynamics of the Upper Ocean, 2nd ed., Cambridge Univ. Press, 1977.
16. Reid, R.O. : Modification of the quadratic bottom-stress law for turbulent channel flow in the presence of surface wind-stress, Technical Memo., No.93, Beach Erosion Board, Corps of Eng., 33p., 1957.
17. Taylor, G.I. : Diffusion by continuous movements, Proc. London Math. Soc., Ser. 2, Vol.20, pp.196-212, 1921.
18. Tsuruya, H., S. Nakano, H. Kato and H. Ichinohe : Experimental study of wind driven currents in a wind-wave tank -Effect of return flow on wind driven currents-, Rept. Port and Harbour Res. Inst., Vol.22, No.2, pp.127-174, (in Japanese).
19. Tsuruya, H., H. Terakawa and Y. Matsunobu : Effects of wind shear and waves on the structure of turbulent streams, Rept. Port and Harbour Res. Inst., Vol.23, No.4, pp.3-70, 1984.
20. van Hoften, J.D.A. and S. Karaki : Interaction of waves and a turbulent current, Proc. 15th Int. Conf. Coastal Engg., Honolulu, pp.404-442, 1976.
21. Zagustin, A. and K. Zagustin : Analytical solution for turbulent flow in pipes, La Houille Blanche, No.2, pp.113-118, 1969.

## APPENDIX - NOTATION

The following symbols are used in this paper:

$A$ = absolute constant ( = 0.47 );

$B_0$ = $\sqrt{|(1-m)r_0-m|}$ ;

$B_1$ = $\sqrt{|1+(1-m)r_1|}$ ;

$C$ = concentration of the property undergoing diffusion;

$D_{i,H}$ = indicator function;

$D_1$ = constant ( = 2.30 );

$D_2$ = constant ( = 1.27 );

$d$ = water depth;

$F$ = flux of the property across a fixed surface;

$f$ = frequency;

$G_{1b}$ = constant ( Eq. 32.a );

$G_{1w}$ = constant ( Eq. 32.a );

$G_{2b}$ = constant ( Eq. 32.b );

$G_{2w}$ = constant ( Eq. 32.b );

$K(T)$ = diffusion coefficient;

$K_x$ = longitudinal diffusion coefficient;

$K_{x0}$ = longitudinal diffusion coefficient in the case of current only;

$K_z$ = vertical diffusion coefficient;

$K_{z0}$ = vertical diffusion coefficient in the case of current only;

$k$ = wave number ( $= 2\pi f/\bar{U}$ );

$k_d$ = ( $= 1/\eta$ ) ;

$\ell$ = mixing length;

$\ell_z$ = mixing length of diffusion in z direction;

$m$ = ratio of bottom stress to surface stress ( $= \tau_b/\tau_s$ );

$N$ = total number of the data used in a computation;

$R$ = radius of the pipe;

${}_wR_E$ = vertical Eulerian auto-correlation coefficient;

${}_wR_L$ = vertical Lagrangian auto-correlation coefficient;

$r$ = radial distance measured from the axis of the pipe;

$r_0$ = relative roughness length for the channel bed ( $= z_{0b}/d$ );

$r_1$ = relative roughness length for the free surface ( $= z_{0w}/d$ );

$S_{i,H}$ = contribution rate from i-th quadrant to the Reynolds stress;

$S(k)$ = wave number spectrum of u component;

$S_0$ = typical power ( $= \varepsilon\nu_w{}^5)^{1/4}$;

$T_{i,H}$ = fraction of time;

$T_L$ = constant time-scale of turbulence;

$U(z)$ = longitudinal current velocity at an elevation z;

$U_a(z)$ = wind speed at an elevation z;

$U_m$ = longitudinal relative current velocity at $\zeta = \zeta_m$ (maximum relative velocity in the case of negative m);

$\bar{U}(z)$ = longitudinal mean velocity at height z;

$\bar{U}_w$ = mean velocity of the section;

$u$ = longitudinal (streamwise) turbulence velocity fluctuations;

$u'$ = longitudinal root-mean-square turbulence-velocity component ( $= \sqrt{\overline{u^2}}$ ) ;

$u_0$ = surface velocity;

$u_*$ = friction velocity of the flow;

$u_{*a}$ = friction velocity of air ( $= \sqrt{\tau_a/\rho_a}$ );

$u_{*b}$ = friction velocity at the bottom ( $= \sqrt{\tau_b/\rho_w}$ );

$u_{*w}$ = friction velocity of the stream at the free surface;

$W(z)$ = vertical current velocity at an elevation z;

$\bar{W}(z)$ = vertical mean velocity;

$w$ = vertical turbulence velocity fluctuations;

$w_L$ = Lagrangian vertical velocity fluctuations;

$w'$ = vertical root-mean-square turbulence-velocity component ( $= \sqrt{\overline{w^2}}$ );

$x$ = holizontal axis;

$y$ = $\sqrt{|m+(1-m)\zeta|}$ ;

$Z$ = vertical displacement of the fluid particle;

$z$ = height above the mean water surface;

$z_{0a}$ = roughness length of water surface for wind;

$z_{0b}$ = roughness length for the channel bed;

$z_{0w}$ = roughness length for the free surface in water;

$\underline{\quad}$ = upper bar denoting overall time average;

$< >$ = conditional sampling;

$\alpha$ = Heisenberg constant in relation to the eddy viscosity;

$\beta$ = ratio of the Lagrangian to Eulerian time scale;

$\beta'$ = assumed value of $\beta$;

$\Delta t$ = data sampling time interval;

$\varepsilon$ = dissipation rate by turbulence per unit mass;

$\zeta$ = relative height measured from the bottom ( = (d+z)/d);

$\zeta_m$ = height at which shear stress vanishes ( = |m| /(1+|m|));

$\eta$ = Kolmogoroff length scale;

$\kappa$ = von Kármán constant ( = 0.4 );

$\kappa'$ = modified von Kármán constant ( = $\kappa(1+r_0+r_1)$);

$\lambda$ = constant ( = 2.0 );

$\lambda_1$ = constant ( Eq. 32.a);

$\lambda_2$ = constant ( Eq. 32.b);

$\lambda_1'$ = constant ( Eq. 32.a);

$\lambda_2'$ = constant ( Eq. 32.b);

$\nu$ = kinematic viscosity of fluid;

$\nu_a$ = kinematic viscosity of air;

$\nu_w$ = kinematic viscosity of water;

$\rho$ = density of fluid;

$\rho_a$ = density of air;

$\rho_w$ = density of water;

$\tau$ = shear stress within the flow;

$\tau_a$ = wind shear stress at the water surface;

$\tau_b$ = shear stress at the bottom; and

$\tau_s$ = shear stress at the free surface.